ACS APPLIED MATERIALS & INTERFACES

Research Article

www.acsami.org

Improved Cyclic Performance of Si Anodes for Lithium-Ion Batteries by Forming Intermetallic Interphases between Si Nanoparticles and Metal Microparticles

Xingkang Huang,[†] Haihui Pu,[†] Jingbo Chang,[†] Shumao Cui,[†] Peter B. Hallac,[‡] Junwei Jiang,[‡] Patrick T. Hurley,[‡] and Junhong Chen*,[†]

[†]Department of Mechanical Engineering, University of Wisconsin-Milwaukee, 3200 North Cramer Street, Milwaukee, Wisconsin 53211, United States

[‡]Global Technology & Innovation, Power Solutions, Johnson Controls, 5757 North Green Bay Avenue, Milwaukee, Wisconsin 53209, United States

Supporting Information

ABSTRACT: Silicon, an anode material with the highest capacity for lithium-ion batteries, needs to improve its cyclic performance prior to practical applications. Here, we report on a novel design of Si/metal composite anode in which Si nanoparticles are welded onto surfaces of metal particles by forming intermetallic interphases through a rapid heat treatment. Unlike pure Si materials that gradually lose electrical contact with conductors and binders upon repeated charging and discharging cycles, Si in the new Si/metal composite can maintain the electrical contact with the current collector through the intermetallic interphases, which are inactive and do not lose physical contact with the conductors and binders, resulting in significantly improved cyclic performance. Within 100 cycles, only 23.8% of the capacity of the pure Si anode is left while our Si/Ni anode obtained at 900 °C maintains 73.7% of its capacity. Therefore, the concept of employing intermetallic interphases between Si nanoparticles and metal particles provides a new avenue to improve the cyclic performance of Si-based anodes.

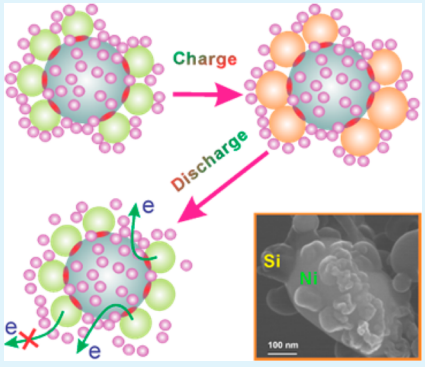

KEYWORDS: *silicon anode, lithium-ion battery, intermetallic interphase, cyclic performance*

INTRODUCTION

Si has high theoretical capacities of 3579 and 4212 mAh g^{-1} at room temperature and high temperatures, respectively, corresponding with the products of $Li_{15}Si_4$ and $Li_{22}Si_5$ observed experimentally.[1−3] Therefore, Si has been investigated extensively as a promising candidate anode for next-generation lithium-ion batteries (LIBs). The most challenging issue for practical applications of Si anodes is to improve their cyclic performance. When Si is charged to $Li_{15}Si_4$, its volume will expand up to 300%. Thus, with repeated cycling, the stress due to large volume expansion often leads to cracking of Si particles and eventually pulverizing of Si, which results in the loss of electrical contact between Si and binders/carbon conductors and thus very poor cyclic performance. For example, a 10 μm Si particle with an initial charge (lithiation) capacity of 3260 mAh g^{-1} only delivered a discharge capacity of 1170 mAh g^{-1} and decayed to ca.100 mAh g^{-1} by the 10th cycle.[4]

Using thin-film Si anodes may improve the cyclic performance;[5−8] however, because of the low Si loading on substrates, it is difficult to use Si thin-film anodes in high-capacity LIBs. Forming Si/carbon composites is believed to be an effective approach to enhance the cyclic performance of Si and has been investigated extensively.[9−16] Carbon is believed capable of serving as a buffering matrix for Si upon lithiation, whereas carbon on the Si surface may also reduce the consumption of electrolytes because of the formation of a solid-electrolyte interphase (SEI) layer on Si. Coating inactive materials on Si surfaces may also improve the cyclic performance of Si.[17−23] However, the coating layer may break during the initial lithiation because of the large volume change, like those observed for SnO_2 anodes by a high-resolution transmission electron microscopy technique.[24] Forming Si/SiO_x composites is another strategy to obtain better cyclic performance, where SiO_x will be reduced by Li to form Li_xO that may act as a matrix for Si expansion upon lithiation;[25−30] however, because of the difficulty in converting Li_xO to Li over a potential range of 0−2 V (vs. Li^+/Li), initial Coulombic efficiencies of Si/SiO_x composites are usually low.

Fabricating Si alloys such as Si−Fe,[31−33] Si−Co,[34] Si−Ni,[35−37] and Si−Al-M (M = Cu, Fe, Mn, Ni, Cr),[38−41] is another approach to improve the cyclic performance while reducing the overall capacity of Si anodes. Basically, forming alloys can reduce the content of active Si, accompanied by consumption of metals to form MSi_x phases (M = Fe,[33] Ni,[36]

Received: August 31, 2013
Accepted: October 21, 2013
Published: October 21, 2013

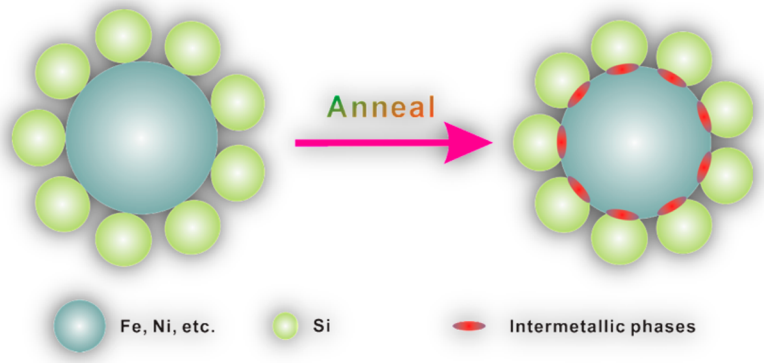

Figure 1. Schematic illustration for fabrication of Si/M composites. Si powders are mixed with metal powders and heat-treated to form intermetallic interphases between Si and metal particles.

Co,[34] Mo,[42] etc.). The decreased total volume change upon lithiation due to reducing the content of active Si, together with the inactive intermetallic matrices to absorb the instantaneous volume change, improves the cyclic performance of Si alloys upon lithiation and de-lithiation. Unlike those reported Si alloys in which the intermetallic phases (MSi_x) work as inactive buffering matrices, in this study, we are using intermetallic phases as a "binder" to weld Si nanoparticles onto surfaces of metal particles (Figure 1). This new composite anode is better than those Si alloys reported in the literature with Si dispersed in inactive MSi_x matrices because the interparticle spacing could effectively accommodate large volume expansion of Si and thus improve the cyclic performance. The Si alloys in the literature typically contain over 50 wt % Si. In contrast, in our design Si/metal (M) composites have a weight ratio of Si/M = 1:3 to obtain a discharge capacity of around 700 mAh g^{-1}, which is sufficient to double the capacity of existing commercial graphite anodes (300−330 mAh g^{-1}) because the capacity of a LIB full cell (18650 type) is primarily limited by the cathode capacity when the anode capacity is beyond 1000 mAh g^{-1}.[1] To form an ideal composite architecture as shown in Figure 1, we control the heat-treatment time for the mixture of nanosized Si and micro-sized M (M = Ni, Cu, Fe, etc.) so that appropriate amount of intermetallic interphases can be produced instead of converting all metals into MSi_x. Details of the experimental section are given in the Experimental Section (see the Supporting Information).

In our design, semiconducting intermetallic phases act as binders to prevent Si from losing electrical contact upon repeated charge/discharge cycles. Because of the large volume change upon charging/discharging (up to ~300% in the form of $Li_{15}Si_4$), for traditional Si anodes, it is inevitable that Si gradually loses electrical contact with binders (such as polyvinylidene fluoride, carboxymethyl cellulose, and poly(acrylic acid)) and conductors (such as carbon black). However, in our design, although the nanosized Si particles may lose their electrical contact with binders and conductors, the metal particles will not because they are inactive and will stay attached to binders and conductors. The Si particles are thus expected to maintain their electrical contact through the intermetallic phases and metals because the latter will not expand and shrink upon charging and discharging. Therefore, such a composite is expected to exhibit good cyclic performance. The selected Si is of an average particle size of 50 nm because Si larger than 150 nm will crack easily upon lithiation.[43] In addition, metals have better electrical conductivities than Si; thus the metals in the composites can improve the electrical conductivity and rate capability of Si anodes.

Figure 2 shows scanning electron microscopy (SEM) images of Ni particles and Si/Ni composites. The employed Ni powder

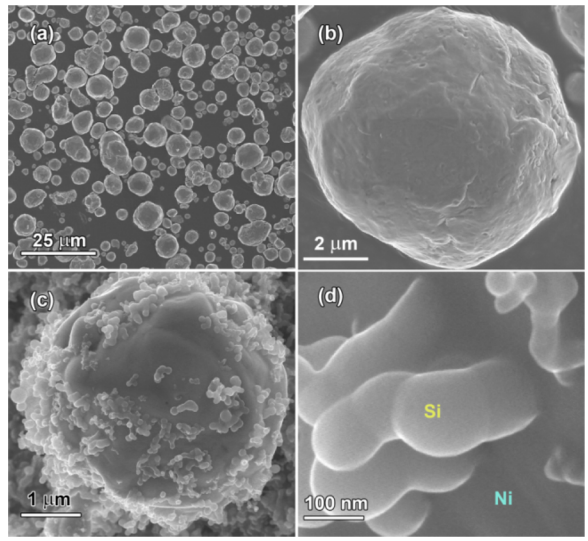

Figure 2. SEM images of (a, b) Ni particles and (c, d) Si/Ni composites obtained at 700 °C; Si particles are seen attached to the surface of an Ni particle.

is composed of spherical Ni particles with a relatively smooth surface (Figures 2a,b). In contrast, in the Si/Ni composite obtained at 700 °C, there are many Si nanoparticles on the surface of Ni particles (Figure 2c). A closer look (Figure 2d) suggests that these Si particles are welded onto the surface of the Ni particle instead of simple physical surface contact between them. Intermetallic phases were detected in this Si/Ni composite by X-ray diffraction (XRD) (see Figure S1 in the Supporting Information). XRD peaks emerging at ca. 25.4 and 45.8° could be indexed to Ni_3Si, Ni_2Si, and $Ni_{31}Si_{12}$. The entropies of formation of these silicides are so close[44] that they are all observed. The content of intermetallic phases increased along with the increasing heating temperature, as indicated by the relative intensities of XRD peaks between silicides and Ni. X-ray photoelectron spectroscopy (XPS) analysis also suggests the existence of silicides on the surface of the Ni/Si composites. For example, the broad XPS peak over a binding energy range

of 850-857 eV for the Si/Ni sample obtained at 900 °C is attributed to Ni metal and nickel silicides (see Figure S2 in the Supporting Information; Ni (852.7 eV), Ni_3Si (852.8 eV), $Ni_{31}Si_{12}$ (853.0 eV), Ni_2Si (853.4 eV), NiSi (853.9 eV), and $NiSi_2$ (854.6 eV)).[45] The morphologies of the Si/Ni composites obtained at 700-900 °C are similar. However, with the sample obtained at 900 °C, we observed much clearer evidence of Si welding onto the surface of Ni particles by SEM plus energy dispersive X-ray spectroscopy (EDS) elemental mapping (Figure 3). When the heating temperature increased

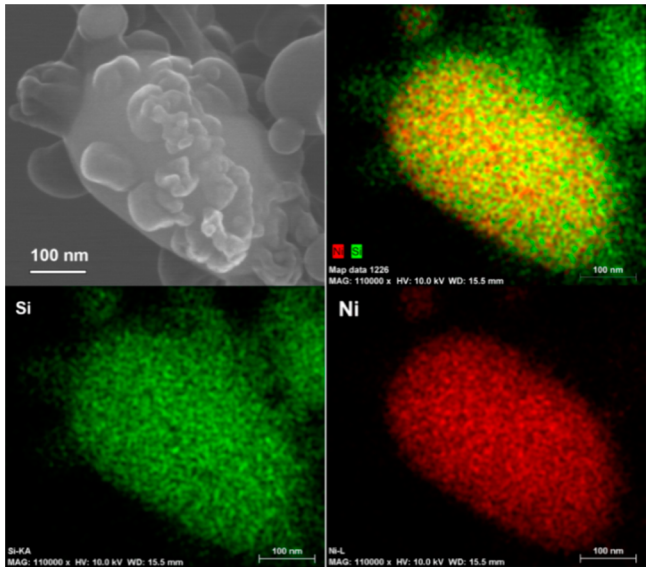

Figure 3. SEM image of the Si/Ni composite synthesized at 900 °C and its corresponding EDS elemental mapping. Note that the images were taken by dispersing the sample in ethanol and then drop-casting onto a 300 mesh copper grid, which helps to eliminate interference from the free Si particles during the EDS analysis.

to 1,000 °C, some beautiful leaf-like surfaces were observed (see Figure S3 in the Supporting Information), which should be silicides. In fact, the content of intermetallic phases in this sample increased significantly compared with those obtained at 700−900 °C as suggested by their relative XRD peak intensities of Si and Ni (see Figure S1 in the Supporting Information).

Pure Si usually possesses very poor cyclic performance, even as nanopowders.[17,46−48] The nanosized Si powders used in our control experiments delivered an initial discharge (delithiation) capacity of 3362 mAh (g Si)$^{-1}$ (Figure 4a); however, the nanosized Si anode decayed very quickly from 2095 mAh (g Si)$^{-1}$ at the 3rd cycle to 498 mAh (g Si)$^{-1}$ by the 100th cycle. Namely, the anode lost an average capacity of about 16.3 mAh (g Si)$^{-1}$ in each cycle. In contrast, our Si/Ni composites showed much better cyclic performance. As shown in Figure 4a, the initial capacities of the Si/Ni composites prepared at 700 and 900 °C are ca. 769 and 626 mAh g^{-1} with initial C.E. of 82.2 and 82.4%, respectively. Note that the specific capacities and current densities were calculated based on the mass of the Si/Ni composites, unless otherwise stated. The highest capacities is 811 and 656 mAh g^{-1}, corresponding with 3244 and 2624 mAh (g Si)$^{-1}$ at the second cycle for the composites obtained at 700 and 900 °C, respectively, because the Si contents in the composites are 25 wt %; when the two composite anodes were charged and discharged at a current density of 233 mA g^{-1}, they delivered ca. 650, 498 mAh g^{-1} and maintained at 474 and 367 mAh g^{-1} by the 100th cycle, namely losing ca. 1.8 and 1.3 mAh g^{-1} each cycle, respectively. Therefore, the cyclic performance of our Si/Ni composites is much better than that of the pristine Si. The Si/Ni composite synthesized at 900 °C has a lower capacity than that of the sample obtained at 700 °C while possessing a better cyclic performance (Figure 4a). This is consistent with the fact that higher heating temperature helps to produce more and thicker intermetallic interphases between Si and Ni.

Considering that Ni has very good electrical conductivity, it may help to obtain a better rate capability compared with pure Si anodes. Figures 4b,c exhibit the rate performance of the Si/Ni composite obtained at 900 °C. At a high current density of 1,400 mA g^{-1} (i.e., 6.4 A (g Si)$^{-1}$), its capacity can reach 227 mAh g^{-1} (i.e., 908 mAh (g Si)$^{-1}$), 34% of the capacity obtained at the small current density of 35 mA g^{-1}. Figure 4d shows CV curves of the Si/Ni composite, recorded at a scan rate of 0.1 mV s^{-1} from an open circuit potential of 3.0 V. During the initial cathodic scan, a current peak emerged at 1.20 V because of the SEI layer formation, followed by a peak at 0.19 V and another developmental peak below 10 mV, corresponding with lithiation of Si to various Li_xSi phases. When potentials were swept anodically, there were two peaks at 0.37 and 0.52 V due to delithiation of Li_xSi. The gradual development of cathodic and anodic peaks is common in CV curves of Si anodes.[46,49,50]

Figure 4e depicts electrochemical impedance spectra (EIS) of the Si/Ni composite in fully charged and discharged states. The Ohmic resistances (including electrolyte and contact resistances) were measured by the intercepts of the Nyquist plots at high frequencies; the values are 2.4 and 1.9 Ohm for the charged and discharged states, respectively. The EIS spectrum in the fully charged state was recorded at 0.183 V with 1 h rest after charging; the obtained spectrum consists of two depressed semi-circles, resulting from the SEI layer and the charge transfer process. The measured resistances are 60.0 and 139.5 Ohm for the SEI layer and the charge transfer process, respectively. We related the depressed semi-circle at high frequencies to the SEI layer because we can also observe this arc in the fully discharged state of this anode; its resistance is 55.9 Ohm, very close to that in the fully charged state. As shown in Figure 4e inset, the impedances in the charged and discharged states are almost the same below 63 Hz, which implies that the anode has a similar SEI layer in the charged and discharged states. However, the second semicircle disappears, accompanied by the appearance of an inclined line, which is very common in the reported literature.[51−54] The inclined line is related to lithium ion diffusion, whereas the depressed semicircle is ascribed to charge transfer resistance[51−53] or combined resistance of SEI and charge transfer.[54] However, we noticed that this Nyquist plot was measured at 1.687 V after allowing the anode to rest for 1 h once it was fully charged to 2.0 V. The charge/discharge curves suggest that the alloying and de-alloying reactions of this anode are below 1.0 V (Figure 4c). Therefore, at such a high voltage of 1.687 V, assuming that the SEI layer is stable, there is no significant reaction since the applied voltage amplitude is only 10 mV. The inclined line should be related to the diffusion of Li ions in the SEI layer instead of in the bulk of Si particles.

The improved cyclic performance is believed to be related to the unique architecture of our designed composite, where the intermetallic interphases help to prevent Si from losing electrical contact with binders and conductors. Figure 5 illustrates the mechanism for improving the cyclic performance of the Si/Ni composite anode. Because of the huge volume

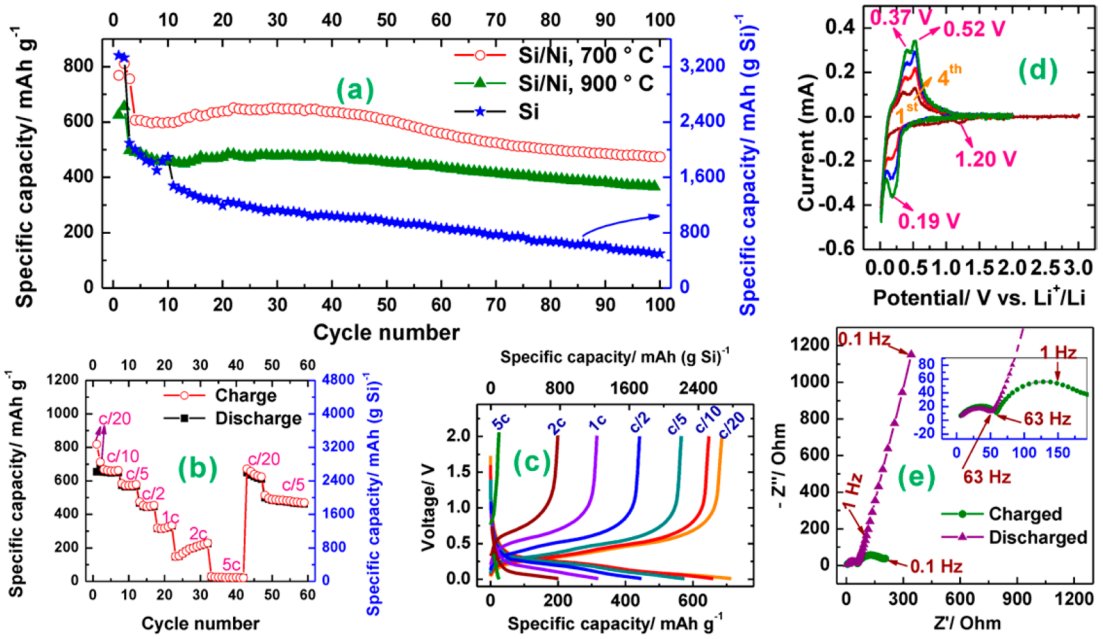

Figure 4. (a) Cyclic performance of the pristine Si and Si/Ni composites obtained at 700 and 900 °C, where the anodes were activated at *C*/20 for 2 cycles and then cycled at 3/*C*; here 1*C* rates were defined as 700 and 2800 mA g^{-1} for the Si/Ni composite and the pristine Si anodes; the current densities are equivalent because the Si content in the composites is 25 wt %. (b–e) Electrochemical performance of the Si/Ni composite prepared at 900 °C: (b, c) rate performance, (d) CV curves at a scan rate of 0.1 mV s^{-1}, and (e) Nyquist plots at fully charged and discharged states.

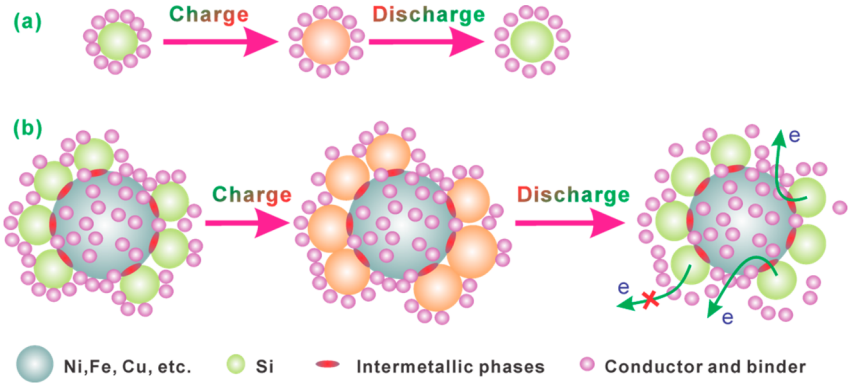

Figure 5. Schematic illustration of (a) degradation mechanism of Si anodes, where Si particles lose electrical contact with conductors and binders upon repeated charging and discharging, and (b) mechanism for the improved cyclic performance of the Si/M composite anodes, where Si particles lose physical contact with conductors and binders, whereas the intermetallic phases and metal particles maintain their electrical contact with conductors and binders because they are inactive and do not expand and shrink upon repeated electrochemical cycles. Note that the particle sizes and their volume changes are not to scale.

change upon repeated charging and discharging, Si particles gradually lose their electrical contact with conductors, binders, and then current collectors, and finally become inactive (Figure 5a). Similarly, the Si particles welded onto the Ni particles via the intermetallic phases lose their physical contact with conductors and binders on the surface of Si; however, the intermetallic phases and Ni particles are inactive and maintain their physical contact with conductors and binders (Figure 5b). Thus, these Si particles welded on the Ni particles could maintain their electrical contact with the current collector through the intermetallic phases and Ni particles. Figure S4 in the Supporting Information shows clear evidence that Si is still attached on the Ni surface and maintains the electrical contact with carbon conductors after 10 cycles of charge and discharge, which suggests that our design can effectively improve the cyclic performance of Si anodes.

The concept of using intermetallic interphases to improve the cyclic performance of Si anodes could be generally employed to synthesize Si/M (M = Ni, Cu, Fe, Co, etc.) composites. In addition to Ni, we also demonstrated the feasibility for Cu and Fe. Figures S5–S7 in the Supporting Information depict the XRD patterns of Si/Cu and Si/Fe composites, where the intermetallic phases of Cu_3Si and Fe_3Si are observed, respectively. The morphologies of the two composites are significantly different from those of the pristine metal particles (see Figures S8 and S9 in the Supporting Information), which also implies the reactions between Si and Cu or Fe. The Si/Cu composite delivered an initial capacity of 801 mAh g^{-1} (i.e., 3,204 mAh (g Si)$^{-1}$) with an initial Coulombic efficiency of 81.8% at 35 mA g^{-1}, and decayed faster than the Si/Ni composite at the current density of 233 mA g^{-1}, namely, from 702 at the 3rd cycle to 381 mAh g^{-1} by the 100th

cycle (see Figure S10 in the Supporting Information). For the Si/Fe composite, its capacity was ca. 487 mAh g^{-1}, and its decaying rates before and after the 50th cycle are 2.2 and 0.51% each cycle, respectively (see Figure S11 in the Supporting Information). Therefore, all the Si/metal composites have better cyclic performance than the pristine Si.

Up to now, there are several reported Si anode materials showing excellent cyclic performance;[15,29] for example, a double-walled Si nanotube consisting of an active silicon nanotube coated with an ion-permeable silicon oxide shell cycled over 6000 times and retained more than 85% of its initial capacity.[29] Admittedly, our Si/metal composites do decay more; for example, the Si/Ni composite retained 73.7% of its reversible capacity after 100 cycles. However, our method of producing the composite anode is low-cost and scalable, and the concept of using intermetallic interphases provides a radically new avenue to improve the cyclic performance of Si materials because our Si/metal composites possess much improved cyclic performance compared with the pure Si anodes. Optimizing particle sizes of Si and metal to increase the fraction of welded Si while reducing the amount of free Si particles is likely a potential strategy to further improve the cyclic performance of the composite anode.

CONCLUSION

In conclusion, we have designed and synthesized low-cost Si/M (M = Ni, Cu, Fe, etc.) composites as anode materials for LIBs, where intermetallic interphases form between Si nanoparticles and metal particles. This new composite anode is better than those Si alloys reported in the literature with Si dispersed in inactive MSi_x matrices; the interparticle spacing could effectively accommodate volume expansion of Si, leading to improved cyclic performance. Moreover, the electrochemically inactive intermetallic interphases in our Si/M (M = Ni, Cu, Fe) composites serve as a special "glue" to prevent Si from losing electrical contact with binders and conductors. The Si/M composites reported here show much better cyclic performance compared with the pure Si anode. For example, the Si/Ni composite synthesized at 900 °C delivered a capacity of 498 mAh g^{-1} at a current density of 233 mA g^{-1} and 73.7% of the capacity remained by the 100th cycle. In contrast, only 23.8% of the capacity of the pure nanosized Si remained after 100 cycles. Therefore, the cyclic performance of Si anodes has been improved significantly through the intermetallic interphases. More importantly, this concept can be generally employed to synthesize various Si/metal composites, where Si could be powders, wires, or films while the metal could be particles, wires, or foil-like substrates such as stainless steel.

ASSOCIATED CONTENT

Supporting Information

Experimental section, additional XRD patterns, XPS analysis, SEM image, EDS elemental mapping, and electrochemical performance. This material is available free of charge via the Internet at http://pubs.acs.org.

AUTHOR INFORMATION

Corresponding Author

*E-mail: jhchen@uwm.edu. Phone: (414) 229-2615.

Notes

The authors declare no competing financial interest.

ACKNOWLEDGMENTS

Financial support for this work was provided by Johnson Controls Inc. The SEM imaging was conducted at the UWM Bioscience Electron Microscope Facility. The authors thank Dr. B. Church and Dr. S. E. Hardcastle for useful discussions on thermal analyses of metals and Si.

REFERENCES

(1) Kasavajjula, U.; Wang, C. S.; Appleby, A. J. *J. Power Sources* **2007**, *163*, 1003−1039.
(2) Key, B.; Bhattacharyya, R.; Morcrette, M.; Seznec, V.; Tarascon, J. M.; Grey, C. P. *J. Am. Chem. Soc.* **2009**, *131*, 9239−9249.
(3) Limthongkul, P.; Jang, Y. I.; Dudney, N. J.; Chiang, Y. M. *Acta Mater.* **2003**, *51*, 1103−1113.
(4) Ryu, J. H.; Kim, J. W.; Sung, Y. E.; Oh, S. M. *Electrochem. Solid-State Lett.* **2004**, *7*, A306−A309.
(5) Yin, J. T.; Wada, M.; Yamamoto, K.; Kitano, Y.; Tanase, S.; Sakai, T. *J. Electrochem. Soc.* **2006**, *153*, A472−A477.
(6) Jeong, H. M.; Lee, S. Y.; Shin, W. H.; Kwon, J. H.; Shakoor, A.; Hwang, T. H.; Kim, S. Y.; Kong, B.-S.; Seo, J.-S.; Lee, Y. M.; Kang, J. K.; Choi, J. W. *RSC Adv.* **2012**, *2*, 4311−4317.
(7) Munao, D.; Valvo, M.; van Erven, J.; Kelder, E. M.; Hassoun, J.; Panero, S. *J. Mater. Chem.* **2012**, *22*, 1556−1561.
(8) Abel, P. R.; Lin, Y. M.; Celio, H.; Heller, A.; Mullins, C. B. *ACS Nano* **2012**, *6*, 2506−2516.
(9) Saint, J.; Morcrette, M.; Larcher, D.; Laffont, L.; Beattie, S.; Peres, J.-P.; Talaga, D.; Couzi, M.; Tarascon, J.-M. *Adv. Funct. Mater.* **2007**, *17*, 1765−1774.
(10) Datta, M. K.; Kumta, P. N. *J. Power Sources* **2007**, *165*, 368−378.
(11) Guo, Z. P.; Milin, E.; Wang, J. Z.; Chen, J.; Liu, H. K. *J. Electrochem. Soc.* **2005**, *152*, A2211−A2216.
(12) Hasegawa, T.; Mukai, S. R.; Shirato, Y.; Tamon, H. *Carbon* **2004**, *42*, 2573−2579.
(13) Holzapfel, M.; Buqa, H.; Scheifele, W.; Novak, P.; Petrat, F. M. *Chem. Commun.* **2005**, 1566−1568.
(14) Wang, W.; Kumta, P. N. *ACS Nano* **2010**, *4*, 2233−2241.
(15) Magasinski, A.; Dixon, P.; Hertzberg, B.; Kvit, A.; Ayala, J.; Yushin, G. *Nat. Mater.* **2010**, *9*, 353−358.
(16) Xin, X.; Zhou, X. F.; Wang, F.; Yao, X. Y.; Xu, X. X.; Zhu, Y. M.; Liu, Z. P. *J. Mater. Chem.* **2012**, *22*, 7724−7730.
(17) Yu, Y.; Gu, L.; Zhu, C. B.; Tsukimoto, S.; van Aken, P. A.; Maier, J. *Adv. Mater.* **2010**, *22*, 2247−2250.
(18) Chen, H.; Xiao, Y.; Wang, L.; Yang, Y. *J. Power Sources* **2011**, *196*, 6657−6662.
(19) Yoshio, M.; Wang, H. Y.; Fukuda, K.; Umeno, T.; Dimov, N.; Ogumi, Z. *J. Electrochem. Soc.* **2002**, *149*, A1598−A1603.
(20) Wang, F.; Xu, S. H.; Zhu, S. S.; Peng, H.; Huang, R.; Wang, L. W.; Xie, X. H.; Chu, P. K. *Electrochim. Acta* **2013**, *87*, 250−255.
(21) Murugesan, S.; Harris, J. T.; Korgel, B. A.; Stevenson, K. J. *Chem. Mater.* **2012**, *24*, 1306−1315.
(22) Lee, J. K.; Yoon, W. Y.; Kim, B. K. *J. Electrochem. Soc.* **2012**, *159*, A1844−A1848.
(23) He, Y.; Yu, X. Q.; Wang, Y. H.; Li, H.; Huang, X. J. *Adv. Mater.* **2011**, *23*, 4938−4941.
(24) Liu, X. H.; Huang, J. Y. *Energy Environ. Sci.* **2011**, *4*, 3844−3860.
(25) Ban, C. M.; Kappes, B. B.; Xu, Q.; Engtrakul, C.; Ciobanu, C. V.; Dillon, A. C.; Zhao, Y. F. *Appl. Phys. Lett.* **2012**, *100*243905.
(26) Iwamura, S.; Nishihara, H.; Kyotani, T. *J. Phys. Chem. C* **2012**, *116*, 6004−6011.
(27) Lee, J. I.; Choi, N. S.; Park, S. *Energy Environ. Sci.* **2012**, *5*, 7878−7882.
(28) Su, L. W.; Zhou, Z.; Ren, M. M. *Chem. Commun.* **2010**, *46*, 2590−2592.
(29) Wu, H.; Chan, G.; Choi, J. W.; Ryu, I.; Yao, Y.; McDowell, M. T.; Lee, S. W.; Jackson, A.; Yang, Y.; Hu, L. B.; Cui, Y. *Nat. Nanotechnol.* **2012**, *7*, 309−314.
(30) Yoo, H.; Lee, J. I.; Kim, H.; Lee, J. P.; Cho, J.; Park, S. *Nano Lett.* **2011**, *11*, 4324−4328.

(31) Lee, H. Y.; Lee, S. M. *J. Power Sources* **2002**, *112*, 649−654.
(32) Dong, H.; Feng, R. X.; Ai, X. P.; Cao, Y. L.; Yang, H. X. *Electrochim. Acta* **2004**, *49*, 5217−5222.
(33) Li, T.; Cao, Y. L.; Ai, X. P.; Yang, H. X. *J. Power Sources* **2008**, *184*, 473−476.
(34) Kim, Y. L.; Lee, H. Y.; Jang, S. W.; Lim, S. H.; Lee, S. J.; Baik, H. K.; Yoon, Y. S.; Lee, S. M. *Electrochim. Acta* **2003**, *48*, 2593−2597.
(35) Lee, H. Y.; Kim, Y. L.; Hong, M. K.; Lee, S. M. *J. Power Sources* **2005**, *141*, 159−162.
(36) Kim, T.; Park, S.; Oh, S. M. *Electrochem. Commun.* **2006**, *8*, 1461−1467.
(37) Wang, Y.; Dahn, J. *J. Electrochem. Soc.* **2006**, *153*, A2314−A2318.
(38) Fleischauer, M. D.; Obrovac, M. N.; Dahn, J. R. *J. Electrochem. Soc.* **2006**, *153*, A1201−A1205.
(39) Liang, P.; Zhang, L.-p.; Wang, F.; Sun, Z.-b.; Hu, Q.; Yang, S.; Wang, L.-q.; Song, X.-p. *Trans. Nonferrous Met. Soc.* **2012**, *22*, 1393−1400.
(40) Zhang, L.; Wang, F.; Liang, P.; Song, X.; Hu, Q.; Sun, Z.; Song, X.; Yang, S.; Wang, L. *Mater. Chem. Phys.* **2011**, *129*, 1006−1010.
(41) Huang, X.; Kim, H.; Cui, S.; Hurley, P. T.; Chen, J. *Energy Technol.* **2013**, *1*, 305−308.
(42) Hwang, C. M.; Lim, C. H.; Yang, J. H.; Park, J. W. *J. Power Sources* **2009**, *194*, 1061−1067.
(43) Liu, X. H.; Zhong, L.; Huang, S.; Mao, S. X.; Zhu, T.; Huang, J. Y. *Acs Nano* **2012**, *6*, 1522−1531.
(44) Acker, J.; Bohmhammel, K. *Thermochim. Acta* **1999**, *337*, 187−193.
(45) Cao, Y.; Nyborg, L.; Jelvestam, U. *Surf. Interface Anal.* **2009**, *41*, 471−483.
(46) Zhao, Y.; Liu, X. Z.; Li, H. Q.; Zhai, T. Y.; Zhou, H. S. *Chem. Commun.* **2012**, *48*, 5079−5081.
(47) Jeong, H. M.; Lee, S. Y.; Shin, W. H.; Kwon, J. H.; Shakoor, A.; Hwang, T. H.; Kim, S. Y.; Kong, B. S.; Seo, J. S.; Lee, Y. M.; Kang, J. K.; Choi, J. W. *RSC Adv.* **2012**, *2*, 4311−4317.
(48) Zhou, X. S.; Yin, Y. X.; Wan, L. J.; Guo, Y. G. *Chem. Commun.* **2012**, *48*, 2198−2200.
(49) Chan, C. K.; Peng, H. L.; Liu, G.; McIlwrath, K.; Zhang, X. F.; Huggins, R. A.; Cui, Y. *Nat. Nanotechnol.* **2008**, *3*, 31−35.
(50) Jiang, T.; Zhang, S. C.; Qiu, X. P.; Zhu, W. T.; Chen, L. Q. *Electrochem. Commun.* **2007**, *9*, 930−934.
(51) Chen, D. Y.; Mei, X.; Ji, G.; Lu, M. H.; Xie, J. P.; Lu, J. M.; Lee, J. Y. *Angew. Chem. Int. Ed.* **2012**, *51*, 2409−2413.
(52) Memarzadeh, E. L.; Kalisvaart, W. P.; Kohandehghan, A.; Zahiri, B.; Holt, C. M. B.; Mitlin, D. *J. Mater. Chem.* **2012**, *22*, 6655−6668.
(53) Ruffo, R.; Hong, S. S.; Chan, C. K.; Huggins, R. A.; Cui, Y. *J. Phys. Chem. C* **2009**, *113*, 11390−11398.
(54) Chen, X. L.; Gerasopoulos, K.; Guo, J. C.; Brown, A.; Wang, C. S.; Ghodssi, R.; Culver, J. N. *Adv. Funct. Mater.* **2011**, *21*, 380−387.